Advances in laser cooling of thulium-doped glass

C. W. Hoyt, M. P. Hasselbeck, and M. Sheik-Bahae

Department of Physics and Astronomy, University of New Mexico, 800 Yale Boulevard NE, Albuquerque, New Mexico 87131

R. I. Epstein, S. Greenfield, J. Thiede, J. Distel, and J. Valencia

Los Alamos National Laboratory, Mail Stop D436, Los Alamos, New Mexico 87545

Received August 9, 2002; revised manuscript received December 9, 2002

Recent developments in cooling thulium-doped heavy-metal fluoride glass are presented. Thulium-doped fluorozirconate (ZBLANP) is cooled to 19 K below ambient with a multiple-pass pump scheme. This represents over an order of magnitude increase from the previously reported single-pass geometry. The results agree with a simple model for anti-Stokes fluorescence cooling that includes considerations of quantum efficiency and parasitic heating mechanisms. Issues relating to a practical optical refrigerator are examined, including a general model for the effects of multiple pump passes. © 2003 Optical Society of America

OCIS codes: 140.3320, 160.5690, 300.2530, 120.6810, 120.3180.

1. INTRODUCTION

Since its first demonstration in 1995,[1,2] laser cooling of matter in the condensed phase has made significant experimental progress. The idea of using radiation to cool such matter was first proposed in 1929 by Pringsheim.[3] Although the notion of using blueshifted fluorescence to decrease the temperature of an object was dismissed by some as contrary to the second law of thermodynamics, Landau established its fundamental validity in 1946.[4] Kastler suggested that rare-earth-doped crystals might provide a medium for solid-state cooling resulting from anti-Stokes emission.[5] Large obstacles stood in the way, primarily the highly efficient heat-generating processes normally associated with absorption in optical materials.

The first solid to cool as a result of interaction with light was a ytterbium-doped fluorozirconate glass.[1] A local decrease in temperature was detected by a photothermal deflection technique when the sample was pumped by a Ti:sapphire laser beam. Bulk cooling was also detected directly from measurements with a calibrated thermally sensitive camera. Thulium-doped glass is the second and only other class of solid to achieve bulk cooling. It was first cooled to 1.2 K below room temperature in 2000;[6] here we report bulk cooling in a thulium-doped fluorozirconate (ZBLANP) to 19 K below room temperature.

Anti-Stokes fluorescence cooling in solids may lead to the development of an all-solid-state cryogenic refrigerator that can be used for a variety of applications. Since 1995, ytterbium-doped glasses have been cooled by nearly 70 K below room temperature and have reportedly cooled at temperatures as low as 77 K.[7] Edwards *et al.* demonstrated a prototypical cryogenic refrigerator based on Yb^{3+}:ZBLANP pumped with a 1.6-W Ti:sapphire laser and measured a temperature decrease of 48 K from room temperature by using a thermocouple.[8] Cooling from low starting temperatures in various Yb^{3+}-doped glasses has been observed, suggesting that a cryogenic refrigerator with an extended dynamic range can be built. Mungan *et al.* observed local cooling in a Yb^{3+}:ZBLANP sample at temperatures between 100 and 300 K, maintaining a cooling efficiency of ~1% throughout this range.[9] Local cooling between 77 K and room temperature by photothermal deflection and spectroscopic techniques in a fluorochloride glass (Yb^{3+}:CNBZn) and in a fluoride glass (Yb^{3+}:BIG) were reported by Fernandez *et al.*[7] The cooling efficiency was shown to change with temperature, varying between ~2% and ~0.6% in the two materials. Rayner *et al.* cooled a Yb^{3+}-doped fiber.[10] Gosnell cooled a Yb^{3+}-doped fiber by an amount $\Delta T = -65$ K from room temperature.[11] The temperature of the fiber was monitored through its temperature-dependent emission spectra. Epstein *et al.* cooled a dielectric-mirrored Yb^{3+}:ZBLANP sample by 70 K from room temperature as measured directly with a thermocouple.

In addition to glasses, ytterbium-doped crystalline samples have been cooled. Crystals offer advantages over glass materials such as high thermal conductivity, improved ruggedness, and potentially larger absorption cross sections. Bowman and Mungan used photothermal deflection to demonstrate local cooling in a Yb^{3+}-doped $KGd(WO_4)_2$ crystal.[12] Epstein *et al.* observed bulk cooling in Yb^{3+}:YAG, recording a net sample temperature change of ~8.9 K below room temperature.[13] They also cooled a sample of Yb^{3+}:Y_2SO_5 by 1 K below room temperature. Mendioroz *et al.* recently showed local cooling in samples of Yb^{3+}:KPb_2Cl_5 crystal.[14]

Optical cooling has been pursued in other condensed-matter materials such as dyes and semiconductors.[15–17] Clark *et al.*[2,18] excited Rhodamine 101 dye with radiation at 1.96 eV and found that it cooled at a rate of 0.7 Kh^{-1}. A GaAs/GaInP heterostructure was studied for possible cooling by Gauck *et al.*[19] They observed blueshifted luminescence but did not see net cooling because coupling inefficiency caused luminescence reabsorption. Finkeißen *et al.* detected local cooling in the area of the-

Table 1. Data Analysis[a]

Sample	Dimensions (mm)	Doping (wt.%)	$\widetilde{\eta_q}$	α_b (cm^{-1})	κ_{fit} (cm K/W)	κ_{calc}
Tm A	$4 \times 4 \times 8$	1	0.99	0.0002	591	825
Tm B	$3 \times 3 \times 10$	2	0.975	0.0004	1002	1224

[a] Tm^{3+}:ZBLANP (ZrF_4-BaF_2-LaF_3-AlF_3-NaF-PbF_2) sample parameters for the $^3H_6 \rightarrow {}^3F_4$ cooling transition. Quantum efficiency ($\widetilde{\eta_q}$), background absorption (α_b), and κ_{fit} are determined when approximation (9) is fit to temperature data. κ_{calc} is determined from Eq. (13).

pump beam spot that was due to anti-Stokes photoluminescence in a GaAs quantum-well structure, recording a temperature drop of 7 K from liquid-nitrogen temperature.[20] As in both of these cases, luminescence trapping that is due to total internal reflection remains a major obstacle to observing net cooling in high-index semiconductor structures.

Here we report progress in laser-induced cooling of thulium-doped glass. Table 1 lists parameters for two cooled samples, including values for quantum efficiency on the cooling transition as discussed in Section 4. A Tm^{3+}-doped ZBLANP sample is irradiated with light from an optical parametric oscillator (OPO) at a wavelength of 1.9 μm causing its temperature to decrease by 19 K from room temperature. Anti-Stokes fluorescence processes in the sample lead to cooling, in part because the dopant–host material combination has high quantum efficiency and the host has low parasitic absorption. Thulium-doped glass cooling systems are shown to be nearly twice as efficient (defined as the ratio of cooling power to absorbed power) as those based on ytterbium, as is expected from pump energy scaling considerations. Further, our results demonstrate anti-Stokes fluorescence cooling in the presence of excited-state absorption, unlike in Yb^{3+}-doped systems.

This paper is organized as follows. In Section 2 we outline a simple derivation of the cooling power possible with anti-Stokes fluorescence. This includes considerations for nonunity external quantum efficiency, parasitic heating mechanisms, and an approximate expression for temperature change in terms of pump power and wavelength. Experiments that demonstrate cooling and the related efficiency scaling are presented in Sections 3 and 4. In Section 5 we discuss multiple-pass optical refrigeration schemes.

2. SIMPLE MODEL OF ANTI-STOKES FLUORESCENCE COOLING IN SOLIDS

The principle of anti-Stokes fluorescence cooling is seen in a description of our particular system. The samples consist of high-purity ZBLANP (in mole percent: 53% ZrF_4, 18% BaF_2, 4-x% LaF_3, 3% AlF_3, 20% NaF, 2% PbF_2, where x is the particular substitution doping value of TmF_3) cut from a fiber preform. The relevant energy manifolds for Tm^{3+} ions in this host are shown in Fig. 1.[21,22] Each level corresponds to a Stark-split manifold of several inhomogeneously broadened levels. We use the transitions between the $^3H_6$ and the $^3F_4$ manifolds for cooling. The cycle leading to anti-Stokes fluorescence cooling involves pump excitation, thermalization, and spontaneous decay. As shown in Fig. 1, laser pump photons excite the dopant ensemble from the top of the ground-state manifold to the bottom of the excited-state manifold. The excitations thermalize within the upper and lower manifolds by absorbing vibrational energy from the host. The atoms decay through spontaneous emission (fluorescence) with a mean photon energy of $h\nu_f$, where ν_f is the mean fluorescent frequency. In the ideal case, for each absorbed pump photon of energy $h\nu$, an average energy $h\nu_f - h\nu$ is removed from the glass and carried out of the system. Cooling power is thus proportional to absorbed power (P_{abs}) and the difference between mean fluorescent and pump photon energies:

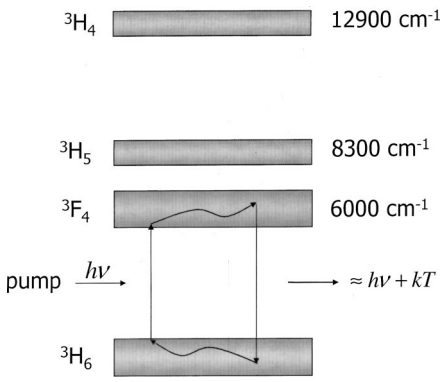

Fig. 1. Energy manifold diagram of Tm^{3+}:ZBLANP, after Refs. 21 and 22. The dopant ensemble is excited by the pump from the top of the ground-state manifold ($^3H_6$) to the bottom of the excited-state manifold ($^3F_4$). The atoms thermalize in both manifolds by absorbing vibrational energy from the host, and the subsequent fluorescence, on average, removes an energy $h\nu_f - h\nu$ for each absorbed photon.

$$P_{cool} = P_{abs}\frac{h\nu_f - h\nu}{h\nu} = P_{abs}\frac{\lambda - \lambda_f}{\lambda_f}, \qquad (1)$$

where λ and $\lambda_f = c/\nu_f$ are the pump and mean fluorescent wavelengths, respectively. Figure 2 shows the room-temperature emission spectrum of a 1-wt. % Tm^{3+}:ZBLANP sample. The spectrum is recorded with an Oriel MS257 monochromater and PbS detector and is corrected for the system response. Also shown is the absorptivity of the sample as taken with a Fourier-transform infrared spectrophotometer (Thermo Nicolet). Defining cooling efficiency as $\eta_{cool} = P_{cool}/P_{abs}$, Eq. (1) yields the fundamental limit on cooling performance. It suggests that, for a given material, longer pump wavelengths produce higher efficiencies. In practice, however, diminished pump absorption at long wavelengths that is due to the thermal distribution of the ground-state population limits the useful maximum pump wavelength.

Moreover, parasitic absorption due to uncontrolled impurities in the material further limits the effective range of long-wavelength excitations. The practical range of the energy difference $h\nu_f - h\nu$ is of the order of thermal energy (k_BT) as a consequence of the ground-state Boltzmann distribution. Therefore Eq. (1) indicates that Tm^{3+}-doped materials with $h\nu_f \approx 0.7$ eV have the potential to cool nearly twice as efficiently as Yb^{3+}-doped materials with $h\nu_f \approx 1.25$ eV.

Although dopant ions with lower-energy gaps can produce more efficient cooling, they will generally be subject to higher nonradiative decay rates that are strongly host dependent. Nonradiative decay in various hosts by multiphonon emission has been shown to exhibit a simple approximate behavior.[23–25] Specifically, the energy-gap law states that the multiphonon emission rate is inversely proportional to the exponential of energy difference (ΔE) between the initial energy state and the energy state below:

$$W_{\mathrm{nr}} = W_0 \exp(-\alpha \Delta E). \tag{2}$$

Here W_0 is a phenomenological parameter that depends strongly on the host material. The parameter a in Eq. (2) is inversely proportional to the characteristic phonon energy in a given material and is thus strongly host dependent. The symbol ΔE in Eq. (2) represents the energy gap of the particular electronic-state transition. Figure 3 is a logarithmic plot of the nonradiative decay rate as a function of energy gap for a number of different hosts.[21,25] In Fig. 3, Eq. (2) was fitted to the data obtained from experiments involving various dopant ions in a given host material. For ZBLAN, the values of W_0 and a are found to be 1.99×10^5 s^{-1} and 0.0021 cm, respectively.[21] The $^3F_4 \rightarrow {}^3H_6$ energy gap in ZBLAN ($\sim$6000 cm^{-1} at the peak of absorption) therefore corresponds to $W_{\mathrm{nr}} = 0.64$ s^{-1}, which is significantly less than the radiative rate of $\sim$83 s^{-1}. The resultant heating that is due to nonradiative processes in pure Tm^{3+}:ZBLANP should be small relative to the cooling processes.

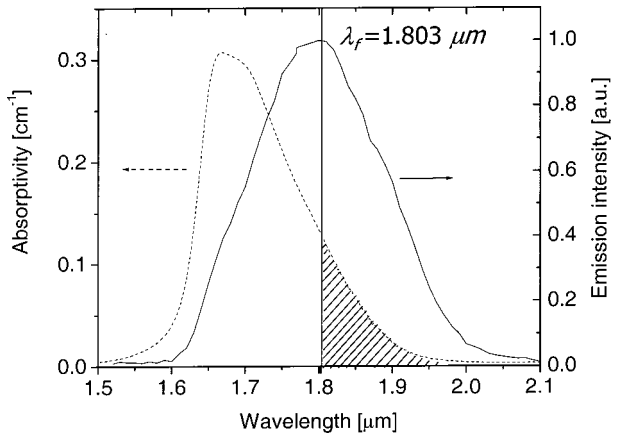

Fig. 2. Absorptivity and fluorescence spectra of 1-wt.% Tm^{3+}:ZBLANP at room temperature. The dotted curve is absorptivity data obtained with a Fourier-transform infrared photospectrometer, and the solid curve is fluorescence data obtained with a monochromater and PbS detector. The vertical solid line marks the mean fluorescent wavelength at 1.803 μm, and the shaded area indicates the pump wavelength region where cooling is expected.

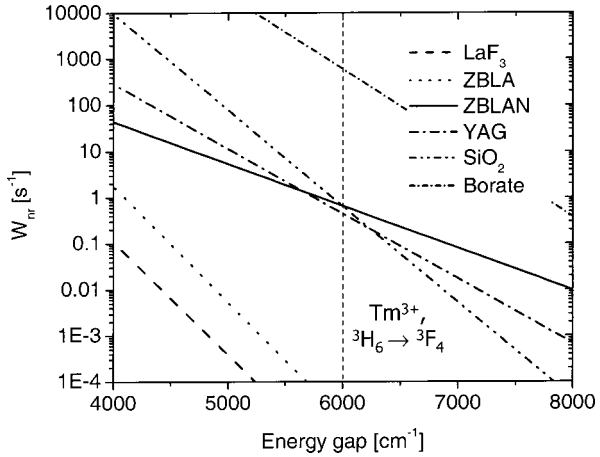

Fig. 3. Nonradiative decay rates versus energy gap for various host materials, after Ref. 21. The vertical dashed line marks the energy gap for the $^3H_6 \rightarrow {}^3F_4$ transition.

Excitations to the $^3H_4$ manifold in Tm^{3+}:ZBLANP have the potential to produce fluorescence cooling. The path $^3H_4 \rightarrow {}^3H_5$ is primarily radiative (see Fig. 3), whereas the $^3H_5 \rightarrow {}^3F_4$ transition is strongly nonradiative. This nonradiative decay can cause heating that would overwhelm the optical cooling effect. Fortunately, the branching ratio for the $^3F_4 \rightarrow {}^3H_5$ transition is 0.03,[25] which indicates that the population of the nonradiative branch should be small. Because the $^3H_4$ manifold lies 6900 cm^{-1} above the $^3F_4$ level, it can be populated by excited-state absorption during illumination by the OPO at 1.85 $\mu m < \lambda < 1.97$ μm. We verified this by observing fluorescence at $\sim$1 μm using a silicon-based video camera. This excited-state absorption process is endothermic and should contribute extra cooling if fluorescence efficiency and background absorption are in the acceptable range. At typical pump wavelengths the absorption cross section for the $^3H_6 \rightarrow {}^3F_4$ transition is $\sim 2 \times 10^{-22}$ cm^2.[25] With a radiative lifetime of 12 ms at a pump wavelength of 1.9 μm, the saturation irradiance is $\sim$84 kW/cm^2. Our average irradiance is less than 10% of this value, so we expect the population of the $^3F_4$ manifold to be much larger than that of the $^3H_4$ manifold. Any heating or cooling effects from the excited-state absorption process should therefore be small relative to the cooling effects on the $^3H_6 \rightarrow {}^3F_4$ transition. We examined transitions to the $^3H_4$ manifold by directly pumping the $^3H_6 \rightarrow {}^3H_4$ transition using a Ti:sapphire laser at 790–900 nm. The sample showed slight heating. This may indicate the presence of strong fluorescence quenching in addition to the processes described above that led to heating.

The amount of cooling power possible in a realistic system can be obtained from a simplified rate-equation model for the $^3H_6$ and $^3F_4$ manifolds:

$$\frac{dN}{dt} = \frac{\mathcal{P}_{\mathrm{abs}}{}^r}{h\nu} - W_{\mathrm{rad}}N - W_{\mathrm{nr}}N + (1 - \eta_e)W_{\mathrm{rad}}N, \tag{3}$$

where N is the number density of excited dopant atoms in the $^3F_4$ manifold, $\mathcal{P}_{\mathrm{abs}}{}^r$ is the resonantly absorbed power density, $h\nu$ is the pump photon energy; and $W_{\mathrm{rad,nr}}$ are the radiative and nonradiative decay rates, respectively. The

last term describes excitations by fluorescence absorbed in transit through the sample. The emitted fluorescence power coupled out of the glass as a fraction of the total generated fluorescence power is $\eta_e \approx 3\{1 - [1 - (1/n)^2]^{1/2}\}\exp[-\alpha_r(\lambda)l]$ for $n > \sqrt{2}$, where n is the index of refraction. The exponential factor accounts for fluorescence reabsorption along a characteristic sample dimension l prior to escape. We obtained this expression by integrating over the cone of fluorescence that satisfies the angular criterion for escape. It assumes that all other totally internally reflected fluorescence is reabsorbed. If $\alpha(\lambda)l \ll 1$, the extraction efficiency is $\eta_e \approx 76\%$ for $n = 1.5$. Estimating an average absorption of $\sim 0.1\ \mathrm{cm}^{-1}$ for the fluorescence spectrum from Fig. 2, this value is further reduced to $\sim 74\%$.

The net laser power density transferred to the sample can be expressed as

$$\mathcal{P}_{\mathrm{net}} = \mathcal{P}_{\mathrm{abs}}{}^{r} + \mathcal{P}_{\mathrm{abs}}{}^{b} - \eta_e N_{\mathrm{ss}} h\nu_f W_{\mathrm{rad}}. \tag{4}$$

Here N_{ss} represents the steady-state number density of excited dopant atoms in the ${}^3F_4$ manifold and $h\nu_f$ is the mean fluorescent photon energy. $\mathcal{P}_{\mathrm{abs}}{}^{b}$ is a nearly wavelength-independent background laser absorption that contributes only to heating. This term corresponds to the background absorption coefficient α_b. The total absorption (α_{total}), which includes α_b, the resonant absorption coefficient $\alpha_r(\nu)$, and any other generalized absorption coefficient (e.g., effective absorption due to scattering losses), attenuates the input laser power such that absorbed power is expressed as $P_{\mathrm{abs}}{}^{i} = P_{\mathrm{in}}(\alpha_i/\alpha_{\mathrm{total}})[1 - \exp(-\alpha_{\mathrm{total}}L)]$. Here P_{in} is the input laser power, L is the physical path length of the beam in the sample, and the index i refers to the particular absorption channel: resonant (r) or background (b).

Combining Eqs. (3) and (4) yields the net power transferred to the sample from the laser radiation:

$$P_{\mathrm{net}} = (P_{\mathrm{in}}\{1 - \exp[-\alpha_{\mathrm{total}}(\nu)L]\}) \times \left[\frac{\alpha_b + (1 - \widetilde{\eta_q})\alpha_r(\nu) - \alpha_r(\nu)\widetilde{\eta_q}\dfrac{h\nu_f - h\nu}{h\nu}}{\alpha_{\mathrm{total}}(\nu)}\right]. \tag{5}$$

A negative net power transferred to the sample in Eq. (5) corresponds to cooling. Here $\widetilde{\eta_q}$ is the external quantum efficiency that accounts for the effect of imperfect fluorescence outcoupling:

$$\widetilde{\eta_q} \equiv \frac{\eta_e W_{\mathrm{rad}}}{\eta_e W_{\mathrm{rad}} + W_{\mathrm{nr}}}. \tag{6}$$

Because $W_{\mathrm{nr}} \approx 0.6\ \mathrm{s}^{-1}$ and $W_{\mathrm{rad}} = 83\ \mathrm{s}^{-1}$, we expect an external quantum efficiency of $\sim 99\%$. Equation (5) indicates that the cooling power is the product of two factors. The term in the bold parentheses is the total absorbed power, and the second term is the cooling efficiency. Expressed such that a positive sign corresponds to cooling, the second term of Eq. (5) can be written as

$$\eta_{\mathrm{cool}} = \widetilde{\eta_q}\frac{\lambda}{\lambda_f}\left[1 + \frac{\alpha_b}{\alpha_r(\lambda)}\right]^{-1} - 1. \tag{7}$$

In the spectral region $\lambda \approx \lambda_f$, the ratio $\alpha_b/\alpha_r(\lambda) \ll 1$, so according to Eq. (7) cooling efficiency should be approximately linear with respect to pump wavelengths in this region. Further, the slope and zero crossing of a plot of $\eta_{\mathrm{cool}}(\lambda)$ are given by $\widetilde{\eta_q}/\lambda_f$ and its inverse, respectively. A measure of quantum efficiency can be made from the pump wavelength at which $\eta_{\mathrm{cool}}(\lambda) = 0$ in this linear region. At this point $\lambda \approx \lambda_f/\widetilde{\eta_q}$. Resonant absorption typically approaches zero for $\lambda \gg \lambda_f$, making $\alpha_b/\alpha_r(\lambda) \gg 1$ for finite α_b. In this case Eq. (7) becomes large in magnitude and negative in sign, indicating significant heating. The ideal efficiency in Eq. (1) is recovered in the limit $\alpha_b = 0$ and $\widetilde{\eta_q} = 1$.

Equation (7) gives a lower limit on the external quantum efficiency allowed in the cooling process for a given pump wavelength. Assuming no background absorption, we see that to exhibit cooling the material must meet the condition

$$\widetilde{\eta_q} > 1 - (k_B T/h\nu_f) \tag{8}$$

if the pump is tuned such that $h\nu_f - h\nu = k_B T$. At room temperature, inequality (8) indicates that cooling is achieved for $\widetilde{\eta_q} > 96.3\%$. This also means that the material must have a nonradiative decay rate less than $2.4\ \mathrm{s}^{-1}$ given the measured value of $W_{\mathrm{rad}} = 83\ \mathrm{s}^{-1}$. According to Fig. 3, the ${}^3F_4 \rightarrow {}^3H_6$ cooling transition in a fluorozirconate host such as ZBLAN or ZBLANP safely meet this criterion, whereas hosts such as borate do not.

Two approximations are helpful in data analysis, both based on measured temperature change. One follows from Eq. (5) and the other from a consideration of thermodynamic factors. In the low pump-depletion limit, such as occurs in a single pass through the sample where $[\alpha_r(\nu) + \alpha_b]L \approx 0.01$, we can express the normalized change in temperature of the sample for small temperature changes as

$$\frac{\Delta T}{P_{\mathrm{in}}} \approx \kappa\left[\alpha_b + \alpha_r(\lambda)(1 - \widetilde{\eta_q}) - \alpha_r(\lambda)\widetilde{\eta_q}\frac{\lambda - \lambda_f}{\lambda_f}\right], \tag{9}$$

where κ is a constant that depends on experimental factors such as radiative load from the surrounding chamber walls and heat conduction to the sample through the physical supports (e.g., glass fibers) and convection from residual gas in the vacuum chamber.

In steady state, the cooling power expressed in Eq. (5) is equal to the external heat load. Assuming negligible conductive and convective loads, the environmental coupling to the sample is radiative. The steady-state cooling power can then be expressed as[18,26,27]

$$P_{\mathrm{cool}} = \frac{1}{1 + \chi}(T_c{}^4 - T_s{}^4)\epsilon_s \sigma A_s, \tag{10}$$

where $T_{s,c}$ correspond to the temperature of the sample and the surrounding chamber, respectively, ϵ_s is the emissivity of the sample, σ is the Stefan–Boltzmann constant, A_s is the sample surface area, and $\chi \equiv (\epsilon_s A_s/\epsilon_c A_c)(1 - \epsilon_c)$ is a ratio involving surface areas and emissivities of the sample and chamber. Equation (10) indicates that well-designed experimental conditions can facilitate low sample temperatures for a given laser cooling power. For example, the sample can be placed in a small chamber

with a surface area approximately equal to its own ($A_s \approx A_c$), and a low-emissivity coating can be designed for the chamber walls such that $\epsilon_c/\epsilon_s \ll 1$. For fluorescence around $\lambda_f = 995$ nm in ytterbium-based cooling systems, such coatings have been shown to reduce radiative load by greater than a factor of 10 relative to a blackbody.[28] Because they do not absorb at longer wavelengths (i.e., 2 μm), these coatings are not adequate for thulium-based refrigerators. Instead we are developing coatings for gold chamber walls based on long-wavelength absorbers PbS or InAs. Without special attention to these issues, nonideal experimental conditions result: $\epsilon_{s,c} \approx 1$ and $A_s/A_c \ll 1$. In this case, for small temperature changes (i.e., $T_s/T_c \approx 1$) Eq. (10) can be written as

$$P_{\text{cool}} \approx 4\sigma A_s T_c^{\,3} \Delta T, \tag{11}$$

where ΔT is the temperature difference between the sample and its surrounding chamber walls. Approximations (9) and (11) characterize the single-pump-pass cooling experiments described in Section 3.

3. EXPERIMENT

A number of Tm^{3+}-doped glasses and crystals (CaF_2, BaF_2, YAlO, LuAG, ZBLANP) are studied, and certain Tm^{3+}:ZBLANP samples exhibit a net cooling effect. The cause of heating in some samples is likely due to both higher effective phonon energies and impurities. Fluorescence quenching and parasitic absorption that are due to unwanted transition metals (e.g., Fe^{2+} or Cu^{2+}) and other rare earths can lead to net heat generation in the sample.

The tunable pump source for our experiments is an OPO based on periodically poled lithium niobate, synchronously pumped by a 25-W cw mode-locked Nd:YAG laser (Coherent Antares). The OPO is operated singly resonant and has a maximum average signal output power of 8 W, signal tunability between 1.75 and 2.05 μm, and a signal output slope efficiency of 46%.[29] See Table 1 for a description of cooled samples. In a cooling experiment the pump beam is focused into the sample, which rests on glass supports (microscope coverslips or fibers) that are in contact with a relatively small surface area and are transparent to the fluorescence. The sample is placed in a vacuum chamber held at $\sim 10^{-5}$ Torr. For experiments with a thermal camera for temperature measurement, an identical reference sample is placed in the chamber on separate supports out of the beam path.

The sample is cooled in both single- and multiple-pass configurations for the pump beam. The former allows us to make high-resolution and precise measurements of sample temperature change with various pump wavelengths, whereas the latter increases the absorbed power. [The effect of increased absorbed power can be seen in the factor of cooling power in bold parentheses in Eq. (5).] For small temperature changes as occur in the single-pass case, we record the net temperature change of the sample relative to the reference sample by using a pyroelectric (ISI Group) or microbolometer-based (Raytheon) thermal camera. The samples are observed through a thermally transparent window (e.g., CaF_2 or NaCl) in the chamber after the sample reaches a steady state with its surroundings inside the vacuum chamber. We calibrate the thermal cameras by controlling the temperature of a similar glass sample. For a particular aperture of the camera, the digitized image yields an 8-bit value that corresponds to the temperature of the sample as read by a reference thermocouple.

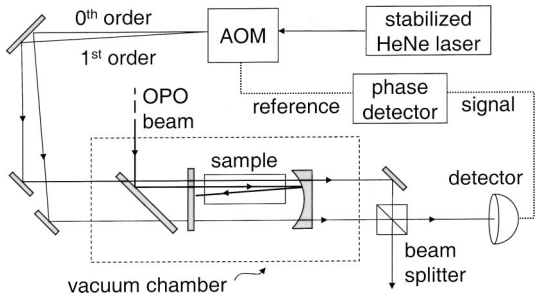

Fig. 4. Diagram of the calibrated Mach–Zehnder heterodyne interferometer used for noncontact temperature measurement. The phase of the 40-MHz beat signal at the detector changes as the sample temperature changes. The interferometer is placed in an enclosure to reduce fluctuations from air movement. AOM, acousto-optic modulator.

In the multiple-pass configuration, the sample is placed on glass supports between two dielectric mirrors of high reflectance ($\sim$99.9%) for the pump beam. The beam passes through a small hole of diameter $\sim$0.4 mm in the dielectric coating of a planar mirror. After the first pass through the sample, the pump beam is reflected from a second dielectric mirror (with a 1-m radius of curvature) back into the sample. The mirrors are optimized such that the beam slightly misses the hole in the first mirror resulting in multiple passes.

The thermal cameras have a resolution of 0.2 K in the range $\Delta T \approx \pm 10$ K from room temperature. To measure larger temperature changes in multiple-pass schemes we instead use a calibrated Mach–Zehnder interferometer. This technique is possible because the optical path length of the sample changes with temperature linearly over a wide range.[30,31] A diagram of the interferometer is shown in Fig. 4. The difference in optical path length between the two arms is defined as $\mathcal{L} = nL - L$ with sample length L and refractive index n. The path lengths through the sample and vacuum are nL and L, respectively. We can then describe the change in path-length difference with respect to sample temperature as

$$\frac{d\mathcal{L}}{dT} = L\left[\frac{dn}{dT} + \beta(n - 1)\right]. \tag{12}$$

Here and below the subscript for sample temperature T_s is omitted. The quantity in brackets describes the material's refractive-index change (dn/dT) and the coefficient of thermal expansion $\beta \equiv 1/L\ dL/dT$. Previously reported values for the bracketed quantity for ZBLAN are -5.9×10^{-6} K^{-1} (Ref. 30) and -5.8×10^{-6} K$^{-1} \pm 0.4$ (Ref. 31). By placing the sample in an optical cryostat (Janis Research) located in the interferometer, we measure the quantity in the brackets in Eq. (12) to be -6.6×10^{-6} K$^{-1} \pm 0.8$ for Tm^{3+}:ZBLANP. This calibration is tested against that of the thermal camera (calibrated against a thermocouple as described above) and found to agree to better than 1 K in the region that the camera is

not saturated. This is well within the resolution of the interferometer (±3 K), which is limited by background phase drifts that occur over time scales of ~1 h.

Heterodyne phase detection schemes can make sensitive measurements of small or rapidly fluctuating phase change.[32–34] As shown in Fig. 4, one arm of the Mach–Zehnder interferometer is shifted by 40 MHz by use of an acousto-optic modulator. When the two beams interfere on the detector, we monitor the phase of the beat signal with respect to the stable 40-MHz acoust-optic modulator reference signal. Signal processing allows phase information to be retrieved with high accuracy. For example, one can use a high-frequency lock-in amplifier that directly displays relative phase.

4. RESULTS AND ANALYSIS

Tables 1 and 2 list the salient results of cooling for the three samples discussed below. The 1-wt.% sample (Tm A) cools in both single- and multiple-pump-pass schemes, and the former results are compared with cooling in 1-wt.% Yb^{3+}:ZBLANP.[1] The 2-wt.% sample (Tm B) cools in a single-pass geometry. Table 1 lists quantum efficiency ($\widetilde{\eta_q}$) and background absorption (α_b) as determined when we fit approximation (9) to temperature data normalized to the incident pump power. Also included in Table 1 are two values for κ [see approximation (9)] determined as follows: (i) κ_{fit} is obtained directly from the data when we fit approximation (9) and (ii) κ_{calc} is found from Eq. (13) discussed below.

Figure 5 shows the induced temperature change in sample Tm B versus the pump wavelength for a single pass of the pump beam. Temperature change is normalized to incident pump power. The insets are false-color thermal images representing sample cooling (bright) and heating (dark). At a pump wavelength of 1.9 μm and an incident average power of ~2.72 W, the sample cools to 2 K below room temperature for a single pass of the pump beam. This corresponds to an absorbed power of ~120 mW. The heating at wavelengths longer than ~1.97 μm can be attributed to parasitic background absorption (α_b) from uncontrolled impurities in the glass such as transition metals. Because absorption in this sample is twice that of Tm A, approximation (9) must be adjusted. Instead of keeping only first-order terms, we use the first four terms in the expansion of the exponential for absorbed power (i.e., the quantity in bold parentheses) in Eq. (5). This form of approximation (9) is indicated by the solid curve in Fig. 5. The sample is found to have an external quantum efficiency $\widetilde{\eta_q} \approx 97.5\%$ and a background absorption $\alpha_b \approx 4 \times 10^{-4}\ \text{cm}^{-1}$. The proportionality constant κ in approximation (9) can be used to evaluate the fidelity of our model. Considering only radiative load to the sample and the steady-state condition $P_{\text{net}} = P_{\text{cool}}$ from Eq. (5) and approximation (11), we obtain

$$\kappa \equiv L/4\epsilon_s A_s T_c^{\,3}. \tag{13}$$

In this relation, L, ϵ_s, and A_s are the sample's length, emissivity, and surface area, respectively. The temperature of the surrounding chamber is T_c, and σ is theStefan–Boltzmann constant. The fit of approximation (9) to the data in Fig. 5 finds $\kappa_{\text{fit}} = 1002$ cmK/W, and

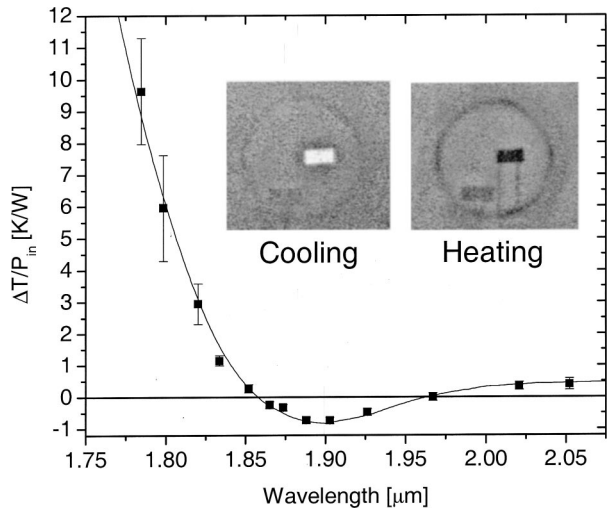

Fig. 5. Temperature change, normalized to incident power, versus pump wavelength for a 2-wt. % Tm^{3+}:ZBLANP sample. The solid curve is a theoretical fit from approximation (9) with $\lambda_f = 1.803\ \mu$m, $\alpha_b = 0.0004\ \text{cm}^{-1}$, and $\widetilde{\eta_q} = 97.5\%$. The insets are thermal images corresponding to different pump wavelengths. Bright areas indicate cooling and dark areas indicate heating.

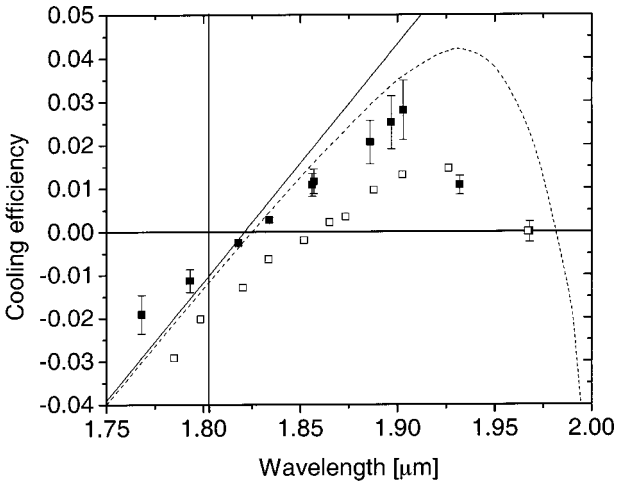

Fig. 6. Cooling efficiency versus pump wavelength for two Tm^{3+}:ZBLANP samples. The solid squares correspond to single-pass data for a 1-wt. % sample, and open squares correspond to a 2-wt. % sample. Error bars are omitted from the open squares for clarity. The solid line corresponds to ideal cooling efficiency adjusted for nonunity external quantum efficiency, and the dashed curve also includes background absorption. The vertical line corresponds to the mean fluorescent wavelength.

Table 2. Rare-Earth Comparison[a]

Sample	Doping (wt.%)	η_{cool} at $h\Delta\nu \sim 1.3\,k_BT$	Slope
Tm A	1	3	2.5
Yb	1	1.5	1.75

[a] Comparison of cooling efficiency at a pump wavelength corresponding to an energy of $\sim 1.3\,k_BT$ from the mean fluorescent wavelength for ZBLANP samples doped with Tm^{3+} and Yb^{3+} ions. Cooling efficiency is indicated in Fig. 7, as is the fitted line.

the value from Eq. (13) is $\kappa_{\mathrm{calc}} = 1224$ cmK/W, which is an 18% difference. For the 1-wt.% sample (Tm A), single-pass cooling data give $\kappa_{\mathrm{fit}} = 591$ cmK/W, which is 28% below the calculated value $\kappa_{\mathrm{calc}} = 825$ cmK/W. These values are listed in Table 1. These values agree within the experimental errors in κ_{fit}, κ_{calc}, and approximation (11).

We can compare the observed cooling efficiencies with the theoretical efficiency of Eq. (7) by using approximation (11) with temperature-change data. Figure 6 shows cooling efficiency ($\eta_{\mathrm{cool}} = P_{\mathrm{cool}}/P_{\mathrm{abs}}$) versus pump wavelength for samples Tm A and Tm B. These data are determined for a given temperature change by the ratio of approximation (11) to absorbed power, assuming unity emissivity for the sample and chamber and neglecting heat load to the sample through conductive or convective channels. The filled squares correspond to the single-pass cooling data of sample Tm A reported in Ref. 6. The solid line is the cooling efficiency given by Eq. (7) with $\lambda_f = 1.803\ \mu$m, $\widetilde{\eta_q} = 99\%$, and $\alpha_b/\alpha_r(\lambda) \ll 1$. The dashed curve in Fig. 6 is obtained when we include the full expression in Eq. (7) (i.e., the addition of both $\widetilde{\eta_q}$ and α_b). The rapid drop in efficiency with increasing pump wavelength is explained by the diminishing resonant absorption that allows background absorption (α_b) to dominate.

The open squares in Fig. 6 indicate cooling efficiency for sample Tm B corresponding to the data in Fig. 5. Error bars similar to those of sample Tm A were omitted for clarity. There is a shifted ordinate intercept and zero crossing and a slightly shifted slope with respect to sample Tm A (solid squares). These shifts offer information about the sample, primarily its external quantum efficiency. We find $\widetilde{\eta_q} \approx 98\%$ for the sample Tm B by fitting Eq. (7) to the data. This estimate is confirmed when we fit approximation (9) to the sample's single-pass normalized temperature data in Fig. 5. Using relation (9), we find $\widetilde{\eta_q} \approx 97.5\%$ and $\alpha_b \approx 4 \times 10^{-4}\ \mathrm{cm}^{-1}$. These values indicate that, even though a higher doping concentration increases absorbed power, this may not necessarily improve cooling. It is well known that higher rare-earth concentrations are related to energy-transfer processes that reduce lifetimes and quantum efficiency.[25,35–40] Sample Tm B has an ~10% reduction in extraction efficiency (η_e) with respect to the lower-doping sample because of increased fluorescence absorption. When we use the same rates as above, Eq. (6) yields $\widetilde{\eta_q} \approx 98.9\%$, which indicates a decrease in extraction efficiency but does not fully account for the observed value of $\widetilde{\eta_q} \approx 97.5\%$. Equation (6) suggests that the nonradiative decay rate increases by a factor of greater than 2, assuming the radiative decay (W_{rad}) remains constant at 83 s^{-1}.

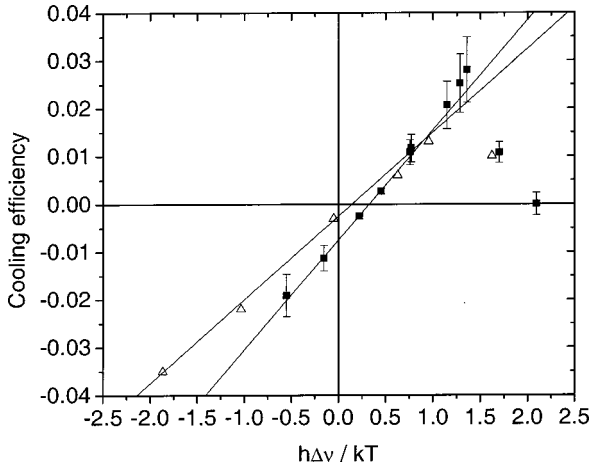

Fig. 7. Cooling efficiency as a function of the pump frequency. The abscissa is the difference of mean fluorescent and pump photon energies as a fraction of room-temperature thermal energy (k_BT). Solid squares correspond to single-pass data for a 1-wt.% Tm^{3+}:ZBLANP sample, and the open triangles correspond to single-pass bulk cooling data obtained by Epstein *et al.* in ytterbium-doped ZBLANP.[1] Slopes are 2.5 and 1.75, respectively. Error bars are omitted for clarity.

Equation (5) and approximation (11) can be used to compare cooling efficiencies in different solid systems. Figure 7 shows cooling efficiency as a function of the pump frequency represented by the ratio of mean fluorescent and pump photon energy difference ($h\nu_f - h\nu$) to thermal energy (k_BT). We compare single-pass cooling data for sample Tm A (solid squares) and ytterbium-doped ZBLANP (open triangles).[1] The slope of thulium cooling efficiency is approximately 50% greater than that of ytterbium. At a pump wavelength corresponding to maximum efficiency in both samples (pump energy ~1.3 k_BT from the mean fluorescent wavelength), Fig. 7 implies that thulium cooling is almost twice as efficient. This suggests that, under identical conditions, a thulium-doped sample should cool nearly twice as much as a ytterbium-doped sample for a given absorbed pump power. Figure 7 directly shows the scale to which these cooling systems are limited by the absorption-related heating effects discussed above. The average difference between mean fluorescent photon energy and pump photon energy is practically limited to ~k_BT in both systems. Table 2 compares cooling efficiency for ZBLANP samples doped with Tm^{3+} and Yb^{3+} ions. Cooling efficiency is determined from Fig. 7, as is the slope of the fitted line.

5. OPTICAL REFRIGERATOR

Cooling power is increased by maximizing absorbed pump power. Because higher doping concentration is ineffective for our system, the term in bold parentheses in Eq. (5) indicates that an increased pump path length can increase the energy removed from the sample. Figure 8 displays data from a cooling experiment in which the pump beam passes multiple times through sample Tm A. Raw data are recorded as phase change in the Mach–Zehnder interferometer, and the corresponding temperature change is obtained through the calibration discussed above. At a time t~10 min, the pump (power ~3.5 W and wavelength 1.9 μm) is coupled into the sample. The sample cools 19 K below room temperature within 25 min. The particular arrangement of the interferometer shown in Fig. 4 leadsto an offset in phase change that is due to the slight difference in path length of the two beams through the second curved mirror as its temperature increases. The time scale of this offset is small with respect to the time to reach steady-state temperature, allowing the offset to be subtracted. The slight oscillations

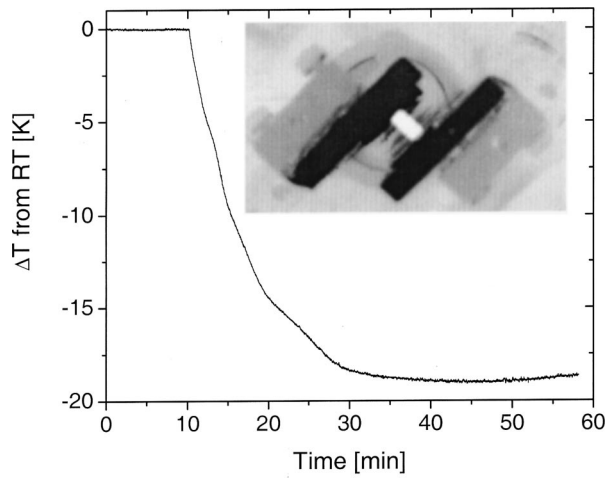

Fig. 8. Cooling data for multiple pump passes through a 1-wt. % Tm^{3+}:ZBLANP sample. Raw data are recorded as phase change in the Mach–Zehnder interferometer. Both the cold sample and the hot mirror mounts can be seen in the inset, which is a thermal image taken from above the experiment. Bright areas correspond to cooling, dark areas correspond to heating. RT, room temperature.

in the phase change data that can be seen in Fig. 8 are also traced to this offset. Both the cold sample and the hot mirror mounts can be seen in the inset, which is a thermal image taken from directly above the experiment. Here the bright regions correspond to temperatures cooler than room temperature, and the dark regions correspond to those warmer than room temperature.

A cryogenic cooler based on anti-Stokes fluorescence requires careful attention to certain practical considerations, including the temperature dependence of cooling efficiency.[7,8,41,42] This factor is an important natural occurrence: For a given pump wavelength in the long-wavelength region of the absorption spectrum, absorption decreases with decreasing temperature because of the decrease in population of the high-lying states in the ground-state manifold according to the Maxwell–Boltzmann distribution. Maximizing the absorbed power seen in the first two factors of Eq. (5) is also an important consideration. This is readily addressed through multiple-pass schemes. Heeg *et al.* have studied the possibility of cooling a sample placed inside a laser resonator operating at the appropriate wavelength.[43] Here we qualitatively consider placing the sample in a nonresonant cavity as described in the experiment above.

For multiple pump passes, the following term multiplies Eq. (5):

$$M = (1 - S^N)/(1 - S). \tag{14}$$

In Eq. (14), N is the number of passes, $S = R \exp(-\alpha_{\text{total}} L)$, α_{total} is the effective absorption of the pump beam, and R is the reflectance of the confining mirrors at each pass. Total absorption includes resonant absorption $[\alpha_r(\lambda)]$ and effective absorption due to scattering (α_s), which accounts for the Fresnel reflections from sample facets, for example. Also included in total absorption is a generalized background absorption that contributes to heating. In Eqs. (5) and (7), α_b is replaced with the generalized background absorption α_b', which includes both the material's fixed background absorption ($\sim 10^{-4}$ cm^{-1} for the experiments above) and any other nearly wavelength-independent heat-generating absorption. This absorption becomes important in samples with mirrors deposited directly on two opposite surfaces. In this case, scattering losses are low and a large number of passes (N) can be achieved. However, absorption in the mirrors can be included in the generalized background absorption (α_b') now present in Eqs. (5) and (7). This can weaken net cooling or even lead to heating. In other words, the factor M in Eq. (14) is effectively maximized when mirrors are deposited directly on the sample, but the potentially large α_b' in Eq. (7) can be detrimental. This is avoided in the case of mirrors external to the sample. Here the effective background absorption is due to the material alone. In this case, however, M is no longer optimized because of finite scattering losses (e.g., Fresnel reflections) and the difficulty of maximizing N.

We have attempted cooling in both of the above cases. Highly reflecting dielectric mirrors are deposited directly on opposite sides of a cylindrical 1-wt.% Tm^{3+}:ZBLANP sample with a radius of ~3 mm, and a small entrance aperture for the pump beam is made in one of the mirrors. After coupling the pump into the sample, we observe heating. Because heating magnitude varies with pump wavelength, the character of the data shows evidence of water absorption in the mirrors. The experiment with external mirrors [see Fig. (8)] shows multiple-pump-pass cooling. In this case we eliminate heating of the sample by the mirrors, but may still optimize the parameters in Eq. (14) by using a sample cut at Brewster's angle, for example.

6. SUMMARY

We have outlined a simple derivation of the cooling power possible with anti-Stokes fluorescence. Included in this are considerations for nonunity external quantum efficiency (related to both lifetime and extraction issues) and parasitic heating mechanisms. Approximate expressions for temperature change enable analysis of single-pass data for two samples. Careful analysis of cooling efficiency gives insight into material properties. Thulium-doped glass has shown almost a factor of 2 increase in cooling efficiency compared with ytterbium-based coolers. A temperature change of −19 K from room temperature is achieved in a multiple-pass geometry, representing an order of magnitude improvement in the cooling of thulium-doped solids with respect to previously reported values. A completely general model for multiple-pass optical refrigeration schemes is developed.

ACKNOWLEDGMENTS

The authors are grateful for assistance from Frank Garcia (University of New Mexico) as well as financial support from the U.S. Air Force Office of Scientific Research (grants F49620-02-1-0059 and F49620-02-1-0057) and the National Aeronautics and Space Administration (grant NAG5-10373). C. W. Hoyt may be reached at hoycha@boulder.nist.gov.

REFERENCES AND NOTES

1. R. I. Epstein, M. I. Buchwald, B. C. Edwards, T. R. Gosnell, and C. E. Mungan, "Observation of laser-induced fluorescent cooling of a solid," Nature **377**, 500–503 (1995).
2. J. L. Clark and G. Rumbles, "Laser cooling in the condensed phase by frequency up-conversion," Phys. Rev. Lett. **76**, 2037–2040 (1996).
3. P. Pringsheim, "Zwei Bemerkungen über den Unterschied von Lumineszenz und Temperaturstrahlung," Z. Phys. **57**, 739–746 (1929).
4. L. Landau, "On the thermodynamics of photoluminescence," J. Phys. (Moscow) **10**, 503–506 (1946).
5. A. Kastler, "Quelues suggestions concernant la production optique et la detection optique d'une mégalité de population des niveaux de quantification spatiale des atomes: application à l'expérience de Stern et Gerlach et à la résonance magnetique," J. Phys. Radium **11**, 255–265 (1950).
6. C. W. Hoyt, M. Sheik-Bahae, R. I. Epstein, B. C. Edwards, and J. E. Anderson, "Observation of anti-Stokes fluorescence cooling in thulium-doped glass," Phys. Rev. Lett. **85**, 3600–3603 (2000).
7. J. Fernandez, A. Mendioroz, A. J. Garcia, R. Balda, and J. L. Adam, "Anti-Stokes laser-induced internal cooling of Yb^{3+}-doped glasses," Phys. Rev. B **62**, 3213–3217 (2000).
8. B. C. Edwards, J. E. Anderson, R. I. Epstein, G. L. Mills, and A. J. Mord, "Demonstration of a solid-state optical cooler: an approach to cryogenic refrigeration," J. Appl. Phys. **86**, 6489–6493 (1999).
9. C. E. Mungan, M. I. Buchwald, B. C. Edwards, R. I. Epstein, and T. R. Gosnell, "Internal laser cooling of Yb^{3+}-doped glass measured between 100 and 300 K," Appl. Phys. Lett. **71**, 1458–1460 (1997).
10. A. Rayner, M. Hirsch, N. R. Heckenberg, and H. Rubinsztein-Dunlop, "Distributed laser refrigeration," Appl. Opt. **40**, 5423–5429 (2001).
11. T. R. Gosnell, "Laser cooling of a solid by 65 K starting from room temperature," Opt. Lett. **24**, 1041–1043 (1999).
12. S. R. Bowman and C. E. Mungan, "New materials for optical cooling," Appl. Phys. B **71**, 807–811 (2000).
13. R. I. Epstein, J. J. Brown, B. C. Edwards, and A. Gibbs, "Measurements of optical refrigeration in ytterbium-doped crystals," J. Appl. Phys. **90**, 4815–4819 (2001).
14. A. Mendioroz, J. Fernández, M. Voda, M. Al-Saleh, and R. Balda, "Anti-Stokes laser cooling in Yb^{3+}-doped KPb_2Cl_5 crystal," Opt. Lett. **27**, 1525–1527 (2002).
15. A. N. Oraevsky, "Cooling of semiconductors by laser radiation," J. Russ. Laser Res. **17**, 471–479 (1996).
16. L. A. Rivlin and A. A. Zadernovsky, "Laser cooling of semiconductors," Opt. Commun. **139**, 219–222 (1997).
17. M. Sheik-Bahae, M. P. Hasselbeck, and R. I. Epstein, "Prospects for laser cooling in semiconductors," in *Quantum Electronics and Laser Science (QELS)*, Postconference Digest, Vol. 74, Trends in Optics and Photonics (Optical Society of America, Washington, D.C., 2002), p. 103.
18. J. L. Clark, P. F. Miller, and G. Rumbles, "Red edge photophysics of ethanolic rhodamine 101 and the observation of laser cooling in the condensed phase," J. Phys. Chem. A **102**, 4428–4437 (1998).
19. H. Gauck, T. H. Gfroerer, M. J. Renn, E. A. Cornell, and K. A. Bertness, "External radiative quantum efficiency of 96% from a GaAs/GaInP heterostructure," Appl. Phys. A **64**, 143–147 (1997).
20. E. Finkeißen, M. Potemski, P. Wyder, L. Vina, and G. Weimann, "Cooling of a semiconductor by luminescence upconversion," Appl. Phys. Lett. **75**, 1258–1260 (1999).
21. L. Wetenkamp, G. F. West, and H. Tobben, "Optical properties of rare earth-doped ZBLAN glasses," J. Non-Cryst. Solids **140**, 35–40 (1992).
22. R. G. Smart, J. N. Carter, A. C. Tropper, and D. C. Hanna, "Continuous-wave oscillation of Tm^{3+}-doped fluorozirconate fibre lasers at around 1.47 μm, 1.9 μm and 2.3 μm when pumped at 790 nm," Opt. Commun. **82**, 563–570 (1991).
23. C. B. Layne and M. J. Weber, "Multiphonon relaxation of rare-earth ions in beryllium-fluoride glass," Phys. Rev. B **16**, 3259–3261 (1977).
24. C. B. Layne, W. H. Lowdermilk, and M. J. Weber, "Multiphonon relaxation of rare-earth ions in oxide glasses," Phys. Rev. B **16**, 10–20 (1977).
25. W. J. Miniscalco, "Optical and electronic properties of rare earth ions in glasses," in *Rare Earth Doped Fiber Lasers and Amplifiers*, M. J. F. Digonnet, ed. (Marcel Dekker, New York, 1993), Chap. 2.
26. R. F. Barron, *Cryogenic Systems, Monographs on Cryogenics*, 2nd ed. (Oxford U. Press, New York, 1985).
27. N. H. Balshaw, *Practical Cryogenics: An Introduction to Laboratory Cryogenics*, 1st ed. (Oxford Instruments, Oxon, England, 1996).
28. B. C. Edwards, M. I. Buchwald, and R. I. Epstein, "Development of the Los Alamos solid-state optical refrigerator," Rev. Sci. Instrum. **69**, 2050–2055 (1998).
29. C. W. Hoyt, M. Sheik-Bahae, and M. Ebrahimzadeh, "High-power picosecond optical parametric oscillator based on periodically poled lithium niobate," Opt. Lett. **27**, 1543–1545 (2002).
30. J. M. Jewell, C. Askins, and I. D. Aggarwal, "Interferometric method for concurrent measurement of thermo-optic and thermal expansion coefficients," Appl. Opt. **30**, 3656–3660 (1991).
31. S. M. Lima, J. A. Sampaio, T. Catunda, A. C. Bento, L. C. M. Miranda, and M. L. Baesso, "Mode-mismatched thermal lens spectrometry for thermo-optical properties measurement in optical glasses: a review," J. Non-Cryst. Solids **273**, 215–227 (2000).
32. T. B. Carlson, S. M. Denzer, T. R. Greenlee, R. P. Groschen, R. W. Peterson, and G. M. Robinson, "Vibration-resistant direct-phase-detecting optical interferometers," Appl. Opt. **36**, 7162–7171 (1997).
33. R. Kristal and R. W. Peterson, "Bragg cell heterodyne interferometery of fast plasma events," Rev. Sci. Instrum. **47**, 1357–1359 (1976).
34. G. M. Robinson, D. M. Perry, and R. W. Peterson, "Optical interferometry of surfaces," Sci. Am. **265**, 66 (1991).
35. It is also possible that higher doping leads to fluorescence quenching because of the concomitant increased impurity concentration.
36. A. Brenier, C. Pedrini, B. Moine, J. L. Adam, and C. Pledel, "Fluorescence mechanisms in Tm^{3+} singly doped and Tm^{3+}, Ho^{3+} doubly doped indium-based fluoride glasses," Phys. Rev. B **41**, 5364–5371 (1990).
37. J. McDougall, D. B. Hollis, and M. J. P. Payne, "Spectroscopic properties of Tm^{3+} in ZBLAN fluoride glass. Part 2. Judd-Ofelt parameters," Phys. Chem. Glasses **36**, 139–140 (1995).
38. M. J. Weber, "Laser excited fluorescence spectroscopy in glass," in *Laser Spectroscopy of Solids*, Vol. 49 of Topics in Applied Physics, 2nd ed. (Springer-Verlag, Berlin, 1986), pp. 189–239.
39. D. L. Huber, "Dynamics of incoherent transfer," in *Laser Spectroscopy of Solids*, Vol. 49 of Topics in Applied Physics, 2nd ed. (Springer-Verlag, Berlin, 1986), pp. 83–111.
40. G. P. Morgan and W. M. Yen, "Optical energy transfer in insulators," in *Laser Spectroscopy of Solids II*, Vol. 49 of Topics in Applied Physics, 1st ed. (Springer-Verlag, Berlin, 1989), pp. 77–122.
41. See Ref. 28; 1.46 W from intracavity to Ti:sapphire laser.
42. G. Lei, J. E. Anderson, M. I. Buchwald, B. C. Edwards, and R. I. Epstein, "Determination of spectral linewidths by Voigt profiles in Yb^{3+}-doped fluorozirconate glasses," Phys. Rev. B **57**, 7673–7678 (1998).
43. B. Heeg, G. Rumbles, A. Khizhnyak, and P. A. DeBarber, "Comparative intra- versus extra-cavity laser cooling efficiencies," J. Appl. Phys. **91**, 3356–3362 (2002).